



Synthesis and characterization of molybdenum complex supported on magnetic and non-magnetic supports: comparing their catalytic activity, selectivity, and reusability

Mojtaba Bagherzadeh¹ · Masomeh Balali² · Mohammad Mehdi Haghdoust¹ · Hassan Keypour³

Received: 20 May 2018 / Accepted: 7 November 2018
© Iranian Chemical Society 2018

Abstract

A molybdenum complex was immobilized on Schiff-base-modified magnetic and non-magnetic particles by covalent linkage. The characterizations of the obtained materials were carried out by means of TG–DTG, SEM, TEM, VSM, XPS, IR, and Raman microprobe techniques. All of them exhibited efficient activities in the oxidation of sulfides to sulfoxides by urea hydrogen peroxide oxidant. The advantages and disadvantages of these catalysts are discussed in detail. Molybdenum complex immobilized on silica bead can be recycled and recovered by simple filtration, but it demonstrated low activity in catalytic oxidation reaction. Immobilization on nano-SiO₂ leads to the formation of nanocatalyst having high catalytic activity but inefficient reusability. The best results were obtained with nano-Fe₃O₄ magnetic support. The immobilized molybdenum complex on silica-coated magnetic nanoparticles can easily be recovered from the reaction system using an external magnet and reused several times with high yields.

Keywords Molybdenum · Supported catalyst · Magnetic · Nanoparticles · Nano-SiO₂

Introduction

The major focus of catalysis research is the enhancing of catalytic activity and recovery. Nowadays, the recovery and reuse of catalysts is become an important factor in “green chemistry” approaches because of their stringent ecological and economical demands for sustainability [1–3]. As a result, from a “green chemist’s” perspective, homogenous catalysts are not environment-friendly [4]. A homogenous catalyst has high activity, but it cannot be easily separated and reused in subsequent reactions. Heterogeneous catalysts

can be recycled and recovered, although their low surface contact leads to a low catalytic activity [5, 6].

One way to increase the active surface of the catalyst is keeping the size of the catalyst particles as small as possible. Therefore, nanoparticles are attractive catalysts, because their large specific surface area can be exploited to achieve high loadings of catalytically active sites. However, nanoparticles with very small size are difficult to separate by typical filtration techniques [7]. In such cases, expensive ultracentrifugation is a most convenient way to nanocatalyst recovery. To circumvent such recycling problems, magnetic nanoparticles (MNPs), which can be easily removed from the reaction mixture by magnetic separation, were recently employed as a catalyst [8–10]. In this respect, over the past decades, the MNPs applications have grown rapidly and have been used for a broad range of catalytic reactions, including oxidations, reductions, hydrogenations, photocatalysis, and C–C bond formations [11–15]. Motivated by these considerations, we have an ongoing interest in the development of new magnetically recyclable nanocatalysts.

It is believed that molybdenum complexes are highly active catalysts for oxidation reaction in the homogeneous and heterogeneous phases [16, 17]. To find the most convenient, effective, and simple heterogeneous Mo-based

Electronic supplementary material The online version of this article (<https://doi.org/10.1007/s13738-018-1545-2>) contains supplementary material, which is available to authorized users.

✉ Mojtaba Bagherzadeh
bagherzadeh@sharif.edu

- ¹ Chemistry Department, Sharif University of Technology, P.O. BOX 11155-3615, Tehran, Iran
- ² Hamedan University of Technology, Hamedan 65155, Iran
- ³ Faculty of Chemistry, Bu-Ali Sina University, Hamedan 65174, Iran

system for the oxidation reaction, the immobilization of Mo(VI) complex on various supports (SiO_2 , nano- SiO_2 , and silica-coated magnetic nanoparticles) is studied in this paper. Since oxidations of sulfides to sulfoxides and sulfones are important chemical reactions found both in nature and industry [18], we chose this reaction as a model reaction to test our designed catalysts.

Experimental

Materials and characterization techniques

Gas chromatographic (GC) analyses were carried out on an Agilent Technology 6890N, 19019J-413 HP-5, 5% phenyl methyl siloxane, capillary 60 m \times 250 μm \times 1 mm. Elemental analyses (C, H, and N) were done using a Heraeus Elemental Analyzer CHN-O-Rapid (Elementar-Analyse systeme, GmbH). Measures of pH were obtained by a Mettler Toledo S40 Seven MultiTM pH meter. Mo content of the catalyst was determined by inductively coupled plasma (ICP) ICP-OES. FT-IR spectra were recorded as KBr pellets using a Perkin Elmer Spectrum Version 10.01.00 spectrophotometer. Scanning electron microscopy (SEM) was performed on Philips XL30. The TGA/DTA curves were determined using 851 Mettler Toledo apparatus. X-ray photoelectron spectroscopy (XPS) was examined by dual anode (Mg and Al $K\alpha$), a chromatic X-ray source. Transmission electron microscopy (TEM) images were obtained on an EM10C (zeiss) transmission electron microscope at an accelerating voltage of 80 kV. Samples dispersed in solution were cast onto a carbon-coated copper grid. Magnetic measurement of materials was investigated with a vibrating sample magnetometer VSM (4 inch, Daghigh Meghnatis Kashan Co., Kashan, Iran) at room temperature. ^1H and ^{13}C NMR spectra were located on a Bruker FT-NMR 500 MHz spectrometer. Raman spectrum was measured by confocal depth profiling with True Focus BRUKER (Germany) equipped with high-energy laser diodes.

Synthesis of 1,4-bis(2-formylphenoxy)methyl benzene (dialdehyde)

The dialdehyde was prepared according to the literature methods [19]. Yield: 0.629 g (58%), m.p. 182 °C, ^1H NMR (500 MHz, CDCl_3): 5.23 ppm (s, 4H, CH_2), 7.11–7.83 ppm (m, 12H, ArH), 10.57 ppm (s, 2H, CHO); ^{13}C NMR (90 MHz, CDCl_3): 189, 160, 140, 135, 128, 127, 126, 121, 113, 71 ppm.

Synthesis of nano- SiO_2

The nano- SiO_2 was synthesized from tetraethyl orthosilicate (TEOS). A mixture of ethanol (2.34 mol), deionized water (18 mL), and $\text{NH}_3\text{-H}_2\text{O}$ (0.01 mol) was stirred vigorously at 50 °C, and dropped with TEOS (0.13 mol) in 1 h. Maintaining reaction at 50 °C for 24 h leads to the formation of nano- SiO_2 [20]. The nanoparticles were centrifuged and washed twice with deionized water. In the next step, they were again centrifuged and finally separated.

Synthesis of $\text{SiO}_2\text{-NH}_2$ and nano- $\text{SiO}_2\text{-NH}_2$

Both $\text{SiO}_2\text{-NH}_2$ and nano- $\text{SiO}_2\text{-NH}_2$ were prepared by the following general procedure. 1 g of SiO_2 (silica gel) or nano- SiO_2 was dispersed in 100 mL of ethanol. Five milliliters of dissolved 3-aminopropyltriethoxysilane (APTS) in 100 mL ethanol were added dropwise to the suspended solid under mechanical stirring. The resultant solid was separated by centrifugation and solid product was suspended in 10 mL of dry methanol [21].

Synthesis of $\text{SiO}_2\text{-SB}$ and nano- $\text{SiO}_2\text{-SB}$

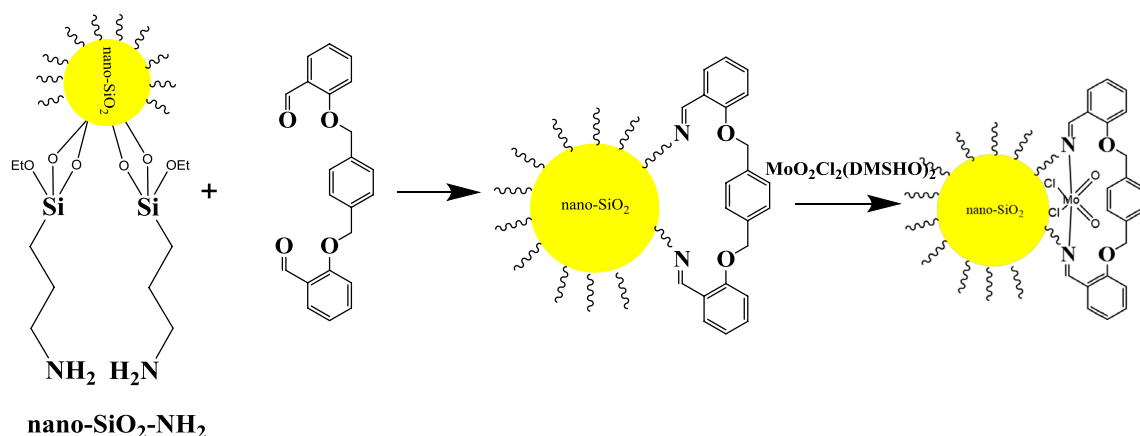
$\text{SiO}_2\text{-SB}$ and nano- $\text{SiO}_2\text{-SB}$ were prepared by the same procedure. A solution of 1,4-bis(2-formylphenoxy)methyl benzene (1 mmol, 0.34 g) in 10 mL dry methanol was added in a dropwise motion to the suspension of $\text{SiO}_2\text{-NH}_2$ or nano- $\text{SiO}_2\text{-SB}$ in dry methanol. The resulted mixture was refluxed for 24 h. The obtained solid was separated by centrifugation and suspended in CH_2Cl_2 (50 mL) for the next synthesis step.

Synthesis of $\text{SiO}_2\text{-SB-Mo(VI)}$ catalyst 1 and nano- $\text{SiO}_2\text{-SB-Mo(VI)}$ catalyst 2

$\text{MoO}_2\text{Cl}_2(\text{DMSO})_2$ (1 mmol, 0.35 g) in 15 mL CH_2Cl_2 was added to the mixture of $\text{SiO}_2\text{-SB}$ or nano- $\text{SiO}_2\text{-SB}$ in CH_2Cl_2 . Then, the mixture was stirred for 24 h under a nitrogen atmosphere. After separation by centrifugation (3000 r min^{-1} in 2 min for $\text{SiO}_2\text{-SB}$ and in 30 min for nano- $\text{SiO}_2\text{-SB}$), the product was washed several times with CH_2Cl_2 to remove unreacted molybdenum precursor (Scheme 1) [22].

Preparation of $\text{Fe}_3\text{O}_4@\text{SiO}_2\text{-NH}_2$ nanoparticles

First, Fe_3O_4 and $\text{Fe}_3\text{O}_4@\text{SiO}_2$ magnetic nanoparticles were prepared according to the reported method [23]. Next, the obtained $\text{Fe}_3\text{O}_4@\text{SiO}_2$ nanoparticles were dried under vacuum and then modified with 3-aminopropyltriethoxysilane (APTS) [24].



Scheme 1 Structures of Schiff base and catalysts 2

Synthesis of Fe₃O₄@SiO₂-SB nanoparticles

1 g of Fe₃O₄@SiO₂-NH₂ was suspended in 10 mL of dry methanol and sonicated for 30 min. Then, a solution of 1,4-bis(2-formylphenoxy)methylbenzene (dialdehyde) (1 mmol, 0.34 g) in 10 mL dry methanol was added in a dropwise motion to the nanoparticles and the resulted mixture was refluxed for 24 h. The resultant solid was separated magnetically and then washed with methanol several times to remove the unreacted residue of the dialdehyde and finally dried under vacuum.

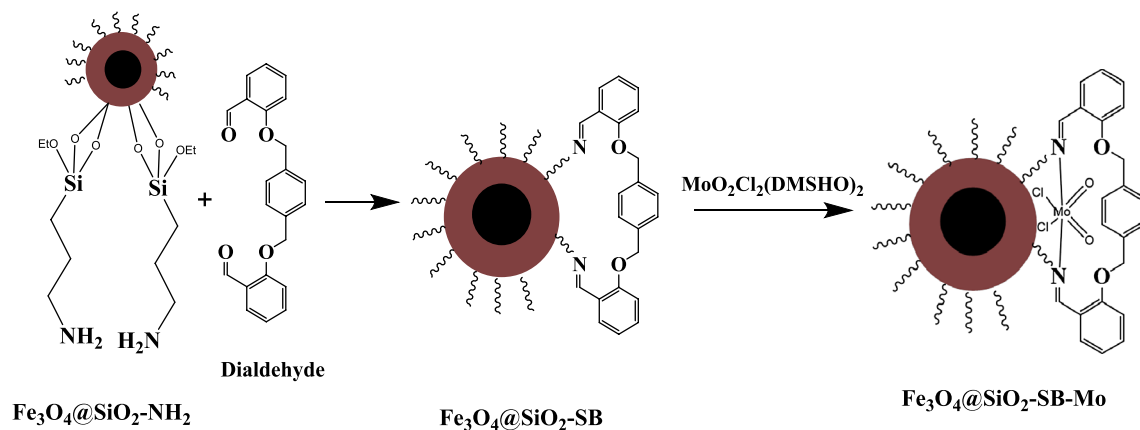
Synthesis of Fe₃O₄@SiO₂-SB-Mo catalyst 3

1 g of Fe₃O₄@SiO₂-SB was sonicated in CH₂Cl₂ (50 ml). Next, MoO₂Cl₂(DMSO)₂ (1 mmol, 0.35 g) in 15 ml CH₂Cl₂ was added and the mixture was stirred for 24 h under a nitrogen atmosphere. After separation with an external magnet,

the product was washed with CH₂Cl₂ to remove unreacted molybdenum precursor (Scheme 2).

General procedure for catalytic oxidation of sulfides

Typically, chlorobenzene (40 mL, 0.4 mmol) as the internal standard and Mo(VI) catalyst (0.01 mmol, calculated by ICP) was added to a solution of sulfide (0.4 mmol) in (1:1) a mixture of CH₃OH-CH₂Cl₂ (1 mL). Then, UHP (0.042 g, 0.45 mmol) as the oxidant was added. The resulting mixture was stirred at room temperature for 30 min. The progress of reaction was monitored by GC (centrifugation was used for separation of non-magnetic catalysts). After magnetic separation of the catalyst, the catalyst was washed with methanol and dichloromethane for several times and used for subsequent cycles [23].



Scheme 2 Structures of Schiff base and catalyst 3

Results and discussion

Synthesis and characterization of catalyst **1**

In the recent years, silica has been receiving much attention as inorganic solid support material for anchoring of metal complexes due to its numerous advantages such as excellent thermal and mechanical stability and economic viability [25]. The synthesis procedure of SiO₂-SB-Mo (catalyst **1**) is represented in Scheme 1. In the first step, the surface of SiO₂ was modified with 3-aminopropyltriethoxysilane (APTS) which created -NH₂ functional group on the SiO₂ surface [26]. Then, SiO₂-NH₂ particles were reacted with 1,4-bis(2-formylphenoxy)methyl) benzenedialdehyde to form surface Schiff-base moiety which can coordinate to the molybdenum center by ligand exchange with DMSO during its treatment with MoO₂Cl₂(DMSO)₂ complex (Scheme 3).

Figure 1 shows the FT-IR spectra of (a) MoCl₂O₂(DMSO)₂ complex, (b) SiO₂-SB, and (c) SiO₂-SB-Mo (catalyst **1**). The FT-IR bands at 1091 cm⁻¹ and 804 cm⁻¹ refer to asymmetric and symmetric stretching vibration of Si-O-Si bond in oxygen-silica tetrahedron, respectively [27]. The absorption band in 1637 cm⁻¹ in FT-IR of SiO₂-SB (Fig. 1b) is ascribed to C=N bonds of Schiff-base group [28]. This band was shifted to higher wavenumber by 30 cm⁻¹ in SiO₂-SB-Mo (Fig. 1c), which indicates coordination of imine group to the Mo(VI) center. In addition, the FT-IR spectrum of the SiO₂-SB-Mo (Fig. 1c) clearly confirmed the formation of molybdenum complex, as exemplified by the appearance of ν(Mo=O) band in 920 and 889 cm⁻¹ [26]. These two bands also exist in the FT-IR spectrum of the unreacted MoO₂Cl₂(DMSO)₂ complex (Fig. 1a). The absorption bands at around 2921 and 2850 cm⁻¹ are due to the stretching vibration of C-H bonds [26].

The thermal behaviors of the catalyst **1** have been studied. TGA experiments were performed under a nitrogen atmosphere with a heating rate of 10 °C per minute in the

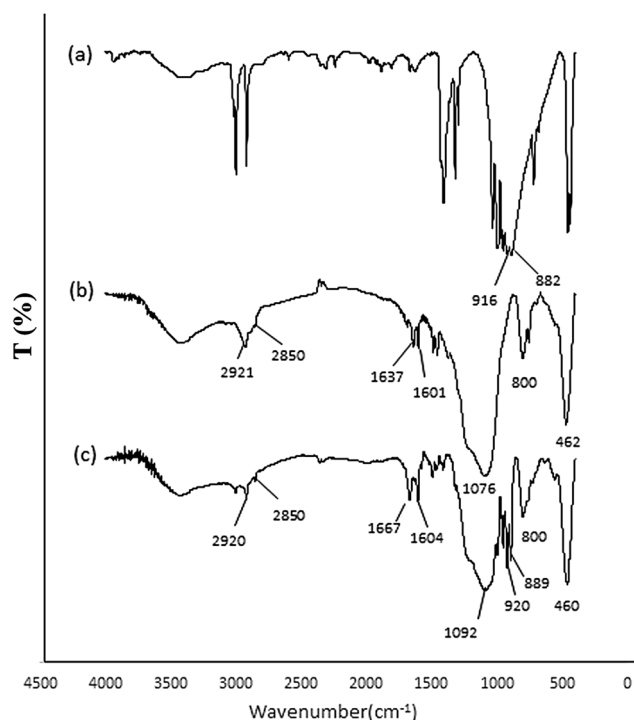
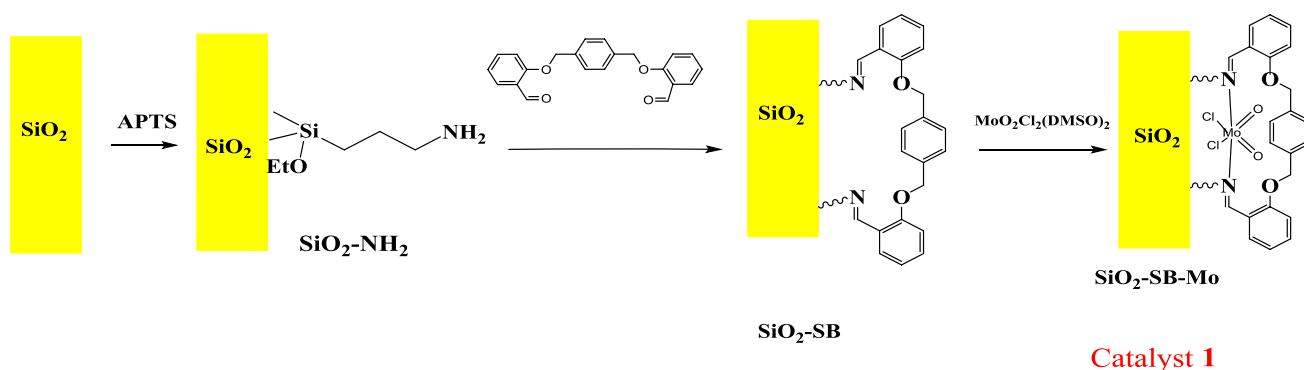
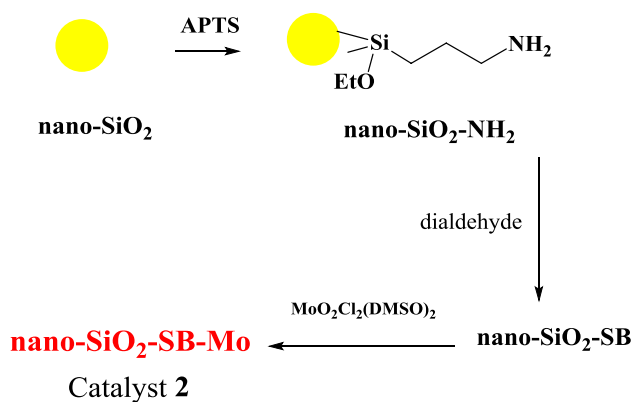
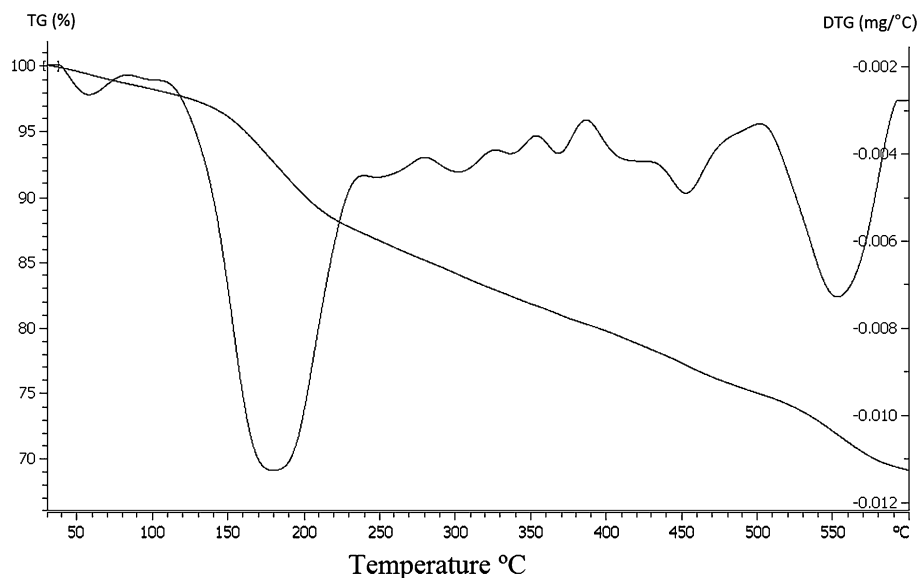


Fig. 1 FT-IR spectra of **a** MoCl₂O₂(DMSO)₂ complex, **b** SiO₂-SB, and **c** catalyst **1**

temperature range 25–600 °C (Fig. 2). The TGA curve of catalyst **1** demonstrated a slow decomposition of the organic part within the range 100–550 °C. At 600 °C, the residual mass percent of catalyst **1** is about 70% [29]. Furthermore, the inductively coupled plasma optical emission spectroscopy (ICP/OES) analysis of the SiO₂-SB-Mo (catalyst **1**) showed 5.667 wt% (0.59 mmol g⁻¹) of Mo content. SEM images of SiO₂ support and catalyst **1** were also provided in supplementary data (Figs. S1 and S2) which can be measured from the images that the particles have the micro-size range diameters (100–200 μm for SiO₂ and 1–20 μm for catalyst **1**).



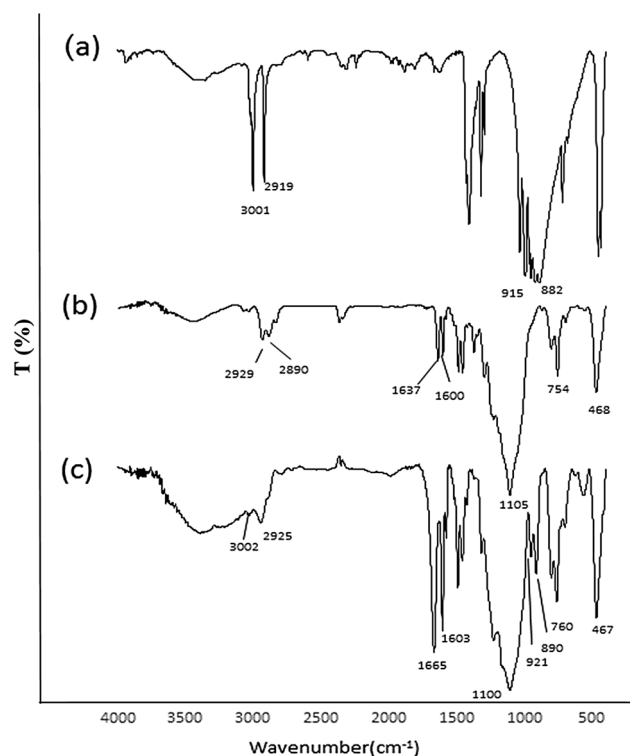
Scheme 3 Step-by-step synthesis of catalyst **1**

Fig. 2 TGA–DTG curve of catalyst **1****Scheme 4** Step-by-step synthesis of catalyst **2**

Synthesis and characterization of catalyst **2**

Comparing to the traditional macro size silica beads, SiO_2 nanoparticles (nano-SiO_2) are more attractive solid support materials, because their large specific surface area can be exploited to achieve high loadings of catalytically active sites [22]. With this idea in mind, Mo(VI) complex was also immobilized on nano-SiO_2 support. The preparation of the $\text{nano-SiO}_2\text{-SB-Mo}$ (catalyst **2**) is very similar to that of catalyst **1** which is indicated as a multistep procedure in Scheme 4. The catalyst **2** was characterized by FT-IR, EDX, SEM, and TGA–DTA analyses.

Like catalyst **1**, the absorption bands of the Si-O-Si group (1100 cm^{-1}), C=N bonds (1665 cm^{-1}), stretching vibration of $-\text{CH}_2$ (3002 and 2925 cm^{-1}), and vibration of Mo=O bonds (921 and 890 cm^{-1}) are seen in FT-IR spectrum of catalyst **2** (Fig. 3c). Comparing the FT-IR spectrum of catalyst **2** with that of $\text{MoO}_2\text{Cl}_2(\text{DMSO})_2$ (Fig. 3a) and

**Fig. 3** FT-IR spectra of **a** $\text{MoCl}_2\text{O}_2(\text{DMSO})_2$ complex, **b** $\text{nano-SiO}_2\text{-SB}$, and **c** catalyst **2**

$\text{nano-SiO}_2\text{-SB}$ (Fig. 3b) confirmed the successful immobilization of $\text{MoO}_2\text{Cl}_2(\text{DMSO})_2$ on nano-SiO_2 nanoparticles.

The chemical identity of nano-SiO_2 and $\text{nano-SiO}_2\text{-SB}$ was confirmed by energy-dispersive X-ray (EDX) analysis (Figs. S3 and S4) [22]. EDX analysis of the $\text{nano-SiO}_2\text{-SB-Mo}$ (catalyst **2**) showed expected elements such as oxygen, silicon, carbon, nitrogen, chlorine, and molybdenum [26].

In addition, the absence of sulfur and the presence of chlorine in EDX analysis revealed that the DMSO ligands in $\text{MoO}_2\text{Cl}_2(\text{DMSO})_2$ complex were completely replaced by surface Schiff-base groups, but the chloride ligand remained unchanged (Fig. 4).

Figure 5a, b shows the SEM image of the nano-SiO₂ and nano-SiO₂-SB-Mo (catalyst 2), respectively. The SEM image indicates that the nano-SiO₂ is composed of spherical nanoparticles. Aggregation leads to increasing the size of observed nanoparticles as seen in the SEM image of catalyst 2 (Fig. 5b) [25]. However, the catalyst 2 particles still fall in the nano-size range.

The thermogravimetric analysis (TGA) curve of the catalyst 2 (Fig. 6) shows the multistep mass loss of the weight between 50 and 600 °C [30]. The weight loss in the first stage (50–120 °C) is due to the releasing of physically adsorbed water and organic solvent. Decomposition of the

organic part is within the range of 120–600 °C. Accordingly, the thermal decomposition in catalyst 2 starts at 120 °C and the residual mass percent is about 40% at 600 °C. In addition, due to the higher surface area of nano-SiO₂ support, a significant increase of the Mo content (10.1 wt%, determined by ICP/OES) was observed for catalyst 2 compared with that of catalyst 1.

Synthesis and characterization of catalyst 3

The small size of nanoparticles complicates that their separation from the reaction mixture and recycling is very difficult. For instance, to separate particles with diameters of less than 100 nm, ultracentrifugation is often the only possibility. To circumvent such recycling problems, magnetic nanoparticles (MNPs), which can be easily removed from the reaction mixture by magnetic separation, were

Fig. 4 Energy-dispersive X-ray spectroscopy (EDX) of the nano-SiO₂-SB-Mo (catalyst 2)

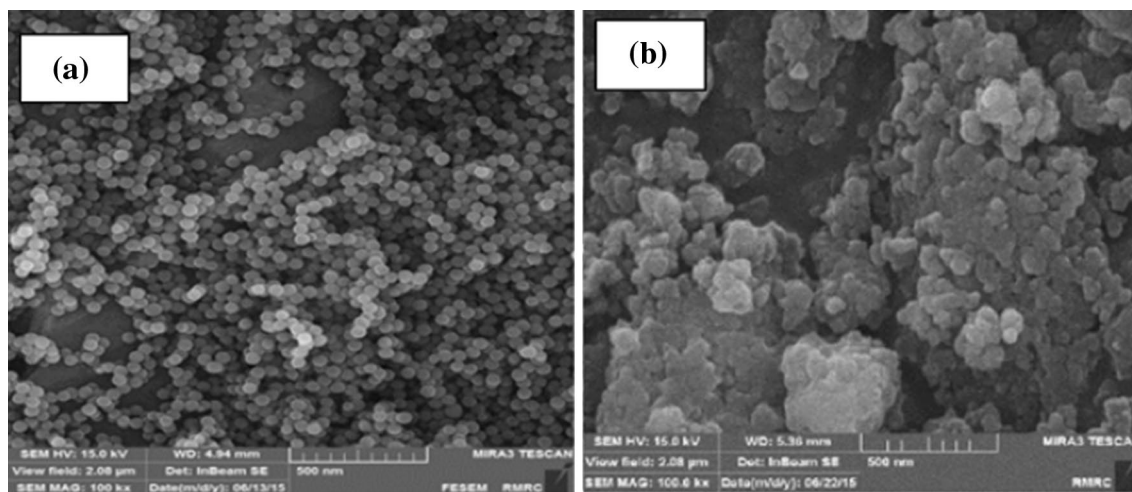
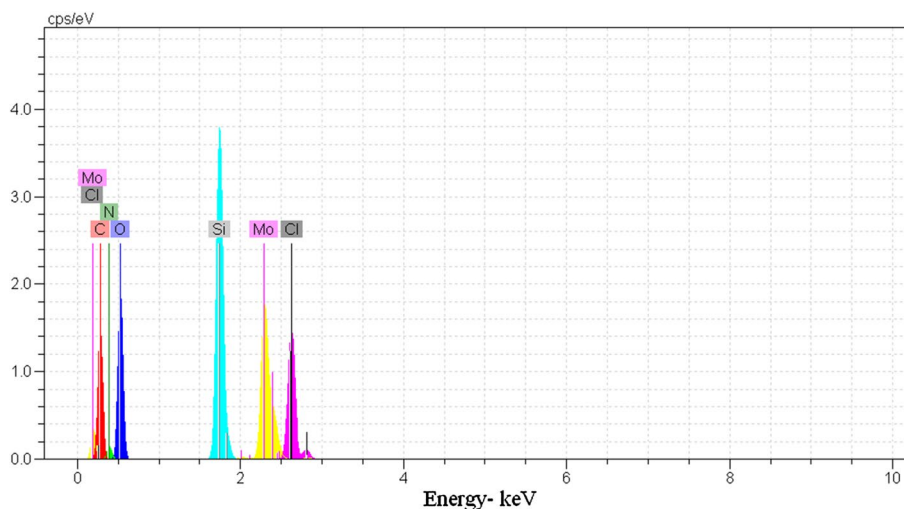
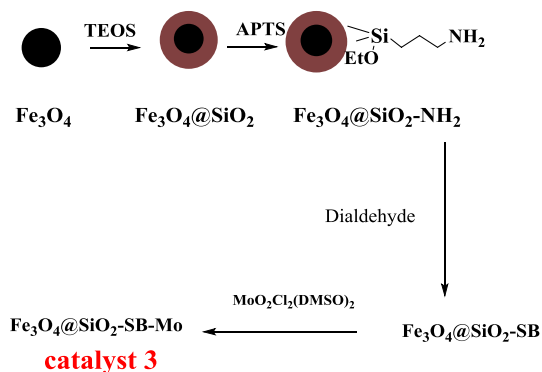
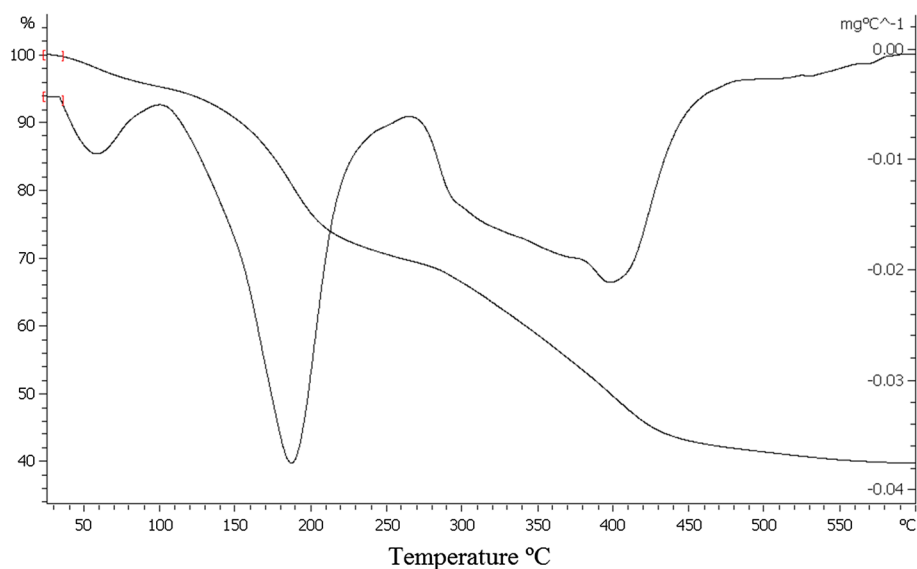
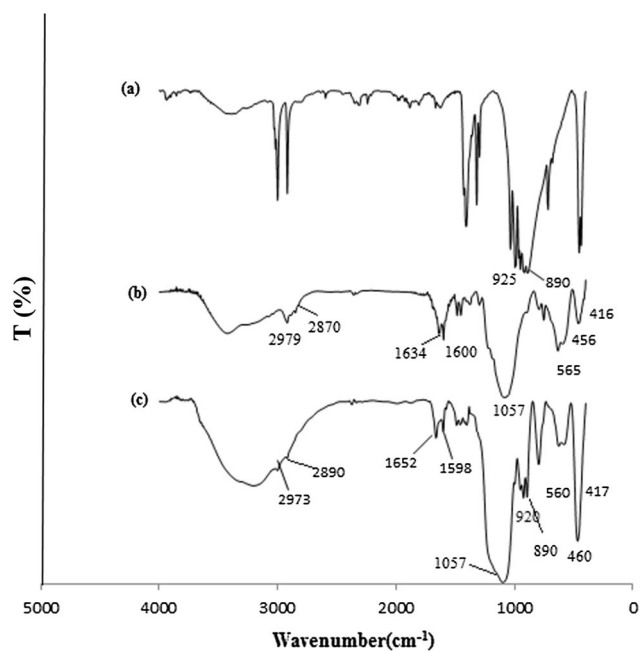


Fig. 5 SEM images of **a** nano-SiO₂ and **b** nano-SiO₂-SB-Mo

Fig. 6 TGA–DTA curve of catalyst **2****Scheme 5** Step-by-step synthesis of catalyst **3**

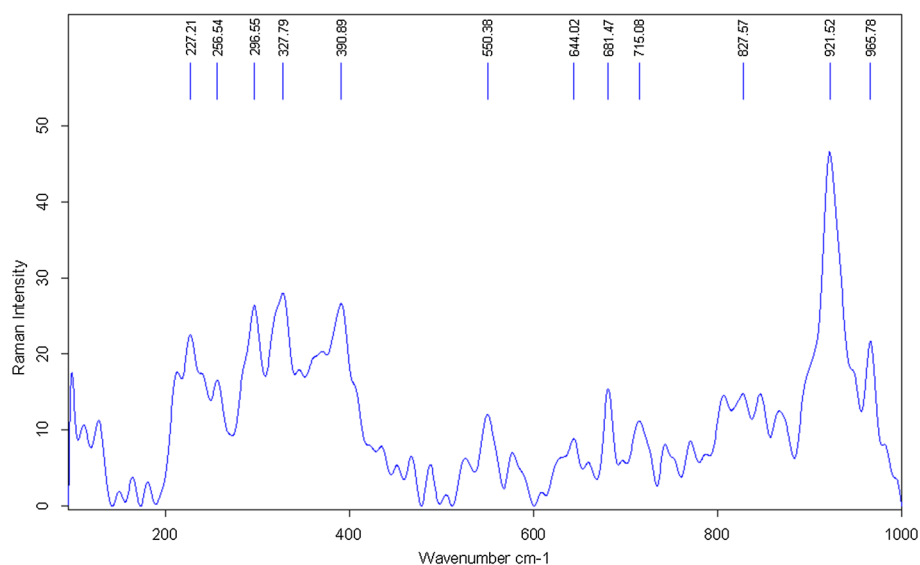
recently employed as a support matrix [4]. Using magnetic nanoparticles, indeed, allows the immobilized catalyst to be removed when the catalytic reaction completed in a simple and efficient way using an external magnet. The size of such magnetic nanoparticles is small enough which showed superparamagnetic behavior. In the other words, they are magnetized in the presence of a magnetic field, but they lost their magnetization as soon as the magnetic field is removed [7]. Thus, in the absence of an external magnetic field, magnetic nanoparticles can efficiently be redispersed in a reaction mixture, providing a large surface area that can be accessed readily by the substrate [31].

Catalyst **3** was prepared by immobilization of $\text{MoO}_2\text{Cl}_2(\text{DMSO})_2$ on the silica-coated MNPs as illustrated in Scheme 5. In the first step, Fe_3O_4 magnetic nanoparticles were prepared by the co-precipitation method [24]. Then, surface of Fe_3O_4 was coated with tetraethyl orthosilicate (TEOS) to increase the functionality and

**Fig. 7** FT-IR spectra of **a** $\text{MoCl}_2\text{O}_2(\text{DMSO})_2$ complex, **b** $\text{Fe}_3\text{O}_4@ \text{SiO}_2\text{-SB}$, and **c** $\text{Fe}_3\text{O}_4@ \text{SiO}_2\text{-SB-Mo}$ (catalyst **3**)

stability of nanoparticles. At the final step, catalyst **3** was synthesized similar to catalyst **1** and **2**.

To confirm the surface modification of the MNPs and the successful formation of the catalyst **3**, FT-IR spectra were provided (Fig. 7). The modified Schiff base, $\text{Fe}_3\text{O}_4@ \text{SiO}_2\text{-SB}$ (Fig. 7b), possesses the peaks at 565 (presence of Fe_3O_4 core) and 1057 cm^{-1} (formation of silica shell) [32]. As mentioned before, the bands in the range of $2800\text{--}2980 \text{ cm}^{-1}$ are related to the C–H stretching vibration of methylene groups (Fig. 7b, c) [33]. The shifted $\nu(\text{C}=\text{N})$ stretch bond of

Fig. 8 Raman spectrum for catalyst **3**

free Schiff-base moiety in $\text{Fe}_3\text{O}_4@\text{SiO}_2\text{-SB}$ from 1634 cm^{-1} to higher frequency 1652 cm^{-1} in the catalyst **3** (Fig. 7c) is due to the coordination of Schiff-base ligands. In addition, appearance of peaks at 920 and 890 cm^{-1} refers to the stretching vibration of $\text{Mo}=\text{O}$ bond in the FT-IR spectrum of catalyst **3** (Fig. 7c) which there are not in the FT-IR spectrum of $\text{Fe}_3\text{O}_4@\text{SiO}_2\text{-SB}$ (Fig. 7b). These bands also exist in the IR spectrum of the unreacted $\text{MoO}_2\text{Cl}_2(\text{DMSO})_2$ complex (Fig. 7a) [19]. All of them prove that Mo(VI) complex is inevitably bonded to the surface of the nanoparticles (Fig. 7b, c).

Figure 8 indicates Raman spectrum (from 200 to 1000 cm^{-1}) of $\text{Fe}_3\text{O}_4@\text{SiO}_2\text{-SB-Mo}$ (catalyst **3**). Raman bands at low wavenumbers (227 and 296 cm^{-1}) are created by the vibrations of Fe-O bonds of iron oxide [34]. The $\text{Fe}_3\text{O}_4@\text{SiO}_2\text{-SB-Mo}$ has a Raman band at around 921 cm^{-1} and 956 cm^{-1} which is related to the stretching mode of the $\text{Mo}=\text{O}$ bond and is considered as an evidence for successful grafting of MoO_2 core [35].

To investigate the morphology of catalyst **3**, SEM and TEM images were provided (Figs. 9, 10) [36]. A large number of nanoparticles with nearly spherical shapes and less than 100 nm dimensions could be found in the TEM and SEM images of sample.

In contrast to the previous TGA–DTA curves of catalyst **1** and catalyst **2**, that of the catalyst **3** (Fig. 11) essentially comprises just one main weight loss step up to $600\text{ }^\circ\text{C}$. The thermal decomposition takes place around $200\text{ }^\circ\text{C}$ and corresponds to the removal of the organic part of nanoparticles [32]. The residual mass percent of catalyst **3** is about 45% at $600\text{ }^\circ\text{C}$.

The chemical identity of Fe_3O_4 , $\text{Fe}_3\text{O}_4@\text{SiO}_2$, and $\text{Fe}_3\text{O}_4@\text{SiO}_2\text{-SB}$ were confirmed by the EDX analysis (Figs. S5, S6, and S7). The EDX analysis of magnetic catalyst **3**

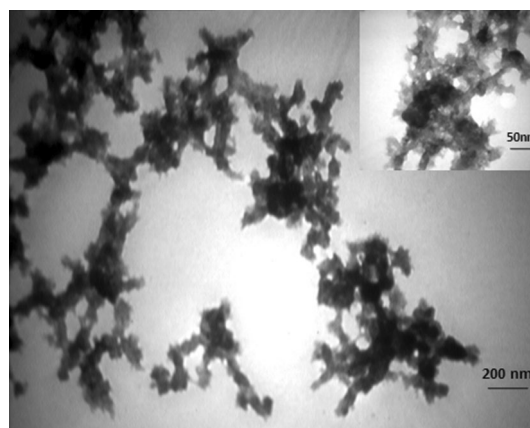
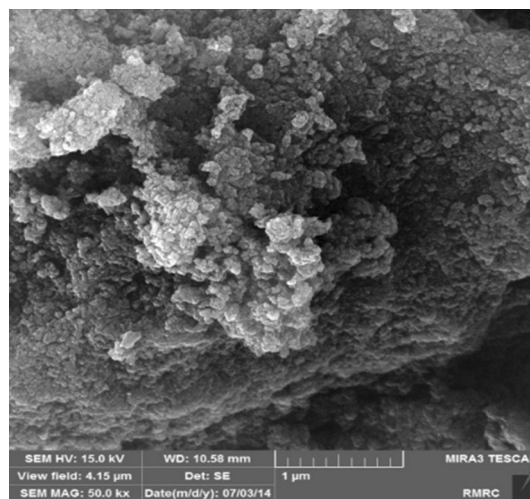
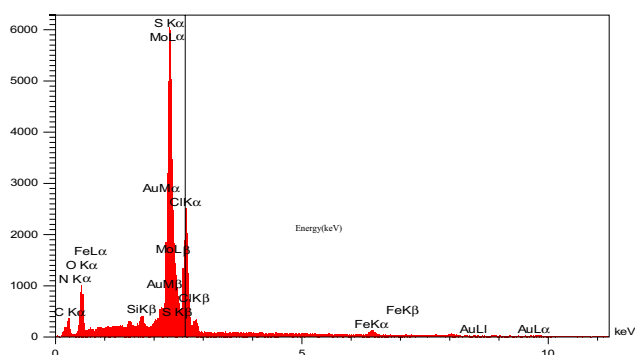
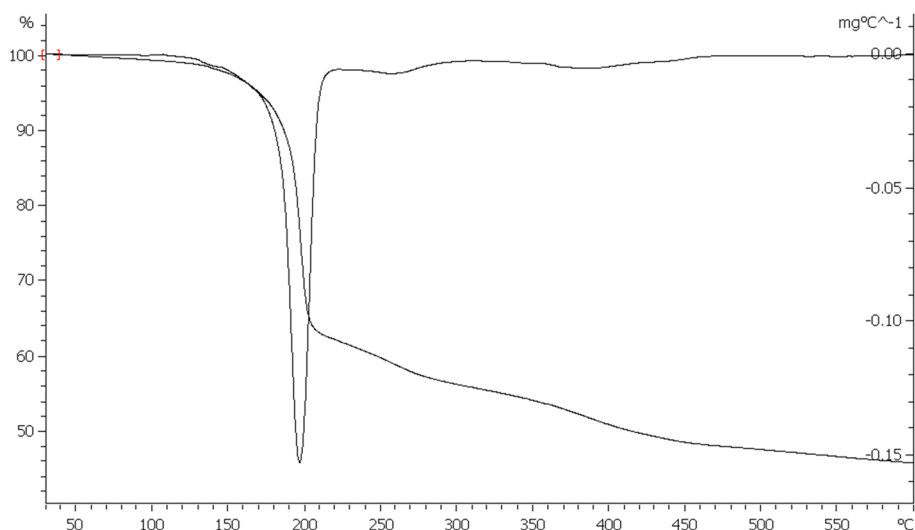
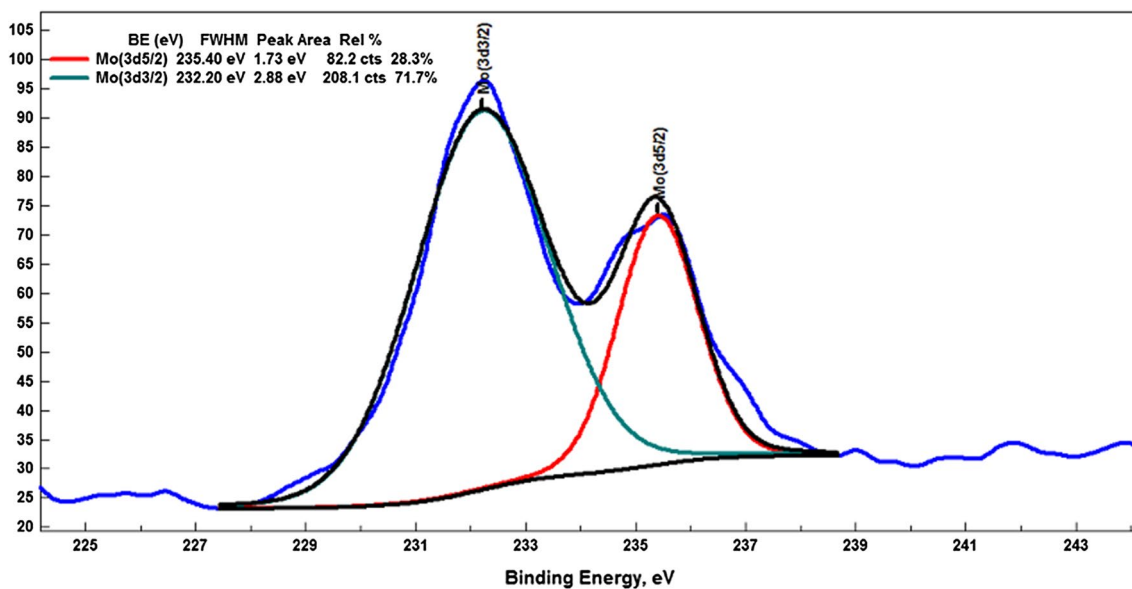
**Fig. 9** TEM images of $\text{Fe}_3\text{O}_4@\text{SiO}_2\text{-SB-Mo}$ (catalyst **3**)**Fig. 10** SEM images of $\text{Fe}_3\text{O}_4@\text{SiO}_2\text{-SB-Mo}$ (catalyst **3**)

Fig. 11 TGA–DTA curve of catalyst **3****Fig. 12** EDX analysis of the catalyst **3**

shows the elements Si, O, C, Fe, Mo, and N, which confirms the expected fabrication of $\text{Fe}_3\text{O}_4@\text{SiO}_2\text{-SB-Mo}$ (Fig. 12) [19]. In addition, the molybdenum content determined from the ICP/OES analysis of the catalyst **3** was about 15.496 wt% (1.63 mmol g^{-1}).

To investigate the chemical states of the elements, X-ray photoelectron spectroscopy (XPS) analyses were performed. Similar to the EDX results, the XPS analysis of the $\text{Fe}_3\text{O}_4@\text{SiO}_2\text{-SB-Mo}$ (catalyst **3**) also revealed expected elements on the surface of nanoparticles such as oxygen, carbon, nitrogen, and molybdenum (Fig. S8). The XPS spectrum in Mo3d region is split into two bands at 232 eV ($3d_{5/2}$) and 235.4 eV

**Fig. 13** Mo3d XPS spectra of the catalyst **3**

($3d_{3/2}$) (Fig. 13). According to the previously reported values in the literature [37, 38], these binding energies are attributed to the Mo in +IV oxidation state. This result confirmed that molybdenum oxidation state remains unchanged during the immobilization on magnetic nanoparticles.

FT-IR, Raman, TEM, SEM, TGA, EDX, and XPS studies provide evidence for anchoring of the Mo(VI) complex. Magnetic measurements of the samples were investigated by a vibrating sample magnetometer (VSM) at room temperature. Based on magnetization curves, the magnetization value decreased from 30 emu g^{-1} in $\text{Fe}_3\text{O}_4@/\text{SiO}_2$ to 4 emu g^{-1} for $\text{Fe}_3\text{O}_4@/\text{SiO}_2\text{-SB-Mo}$ (Fig. 14). This drop in saturation magnetization value is due to the presence of non-magnetic silica phase, organic Schiff-base group, and molybdenum complex around the Fe_3O_4 magnetic core [33].

Catalytic activity

Sulfoxides are known because of having interesting and useful biological and pharmacodynamic properties [22, 28, 29]. The main synthetic route for the preparation of the sulfoxides is via selective oxidation of the corresponding sulfides. The catalytic activities of catalyst **1** (silica support), **2** (nano-silica support), and **3** (nano-magnetic support) were investigated in the chemoselective oxidation of sulfides to sulfoxides using urea hydrogen peroxide (UHP) as oxidant. Initially, the efficiency of three catalysts was compared according to their results on the oxidation of methyl phenyl sulfide (Table 1). As can be observed in Table 1, the catalytic efficiency increased along the series

Table 1 Oxidation of methyl phenyl sulfide by catalyst **1**, **2**, and **3** in the presence of UHP oxidant

Catalysts	Time (min)	Conversion (%) ^a	Selectivity (%) ^b
1	30	67	95
1	60	76	72
2	30	82	100
2	60	> 99	96
3	30	> 99	95

Reaction condition: sulfide (0.4 mmol), UHP (0.45 mmol), catalyst (0.01 mmol of molybdenum content), 0.5 mL CH_2Cl_2 , 0.5 mL MeOH, room temperature

^aDetermined by GC using chlorobenzene as an internal standard

^bDetermined by GC, selectivity to sulfoxide = $[\text{sulfoxide \%}/(\text{sulfoxide \%} + \text{sulfone \%})] \times 100$

1 < **2** < **3**. As was predictable, comparative catalytic study revealed the superiority of nano-size catalysts **2** and **3** over micro-size catalyst **1**. In this case, nano-nature of support provides a large surface area for catalyst **2** and **3** which can be accessed readily by the substrate. Also control experiments indicated that no oxidation occurred in the absence of either nanocatalysts or oxidant. In addition, the use of SiO_2 , $\text{SiO}_2\text{-NH}_2$, $\text{Fe}_3\text{O}_4@/\text{SiO}_2$, or $\text{Fe}_3\text{O}_4@/\text{SiO}_2\text{-NH}_2$ nanoparticles and SiO_2 , $\text{SiO}_2\text{-NH}_2$ in place of nanoparticles did not promote oxidation.

Catalyst **1** can be easily recycled and reused for five successive catalytic cycles by simple filtration (Fig. 15). However, the catalytic activity of catalyst **2** was significantly reduced in the second and third cycles (from 99

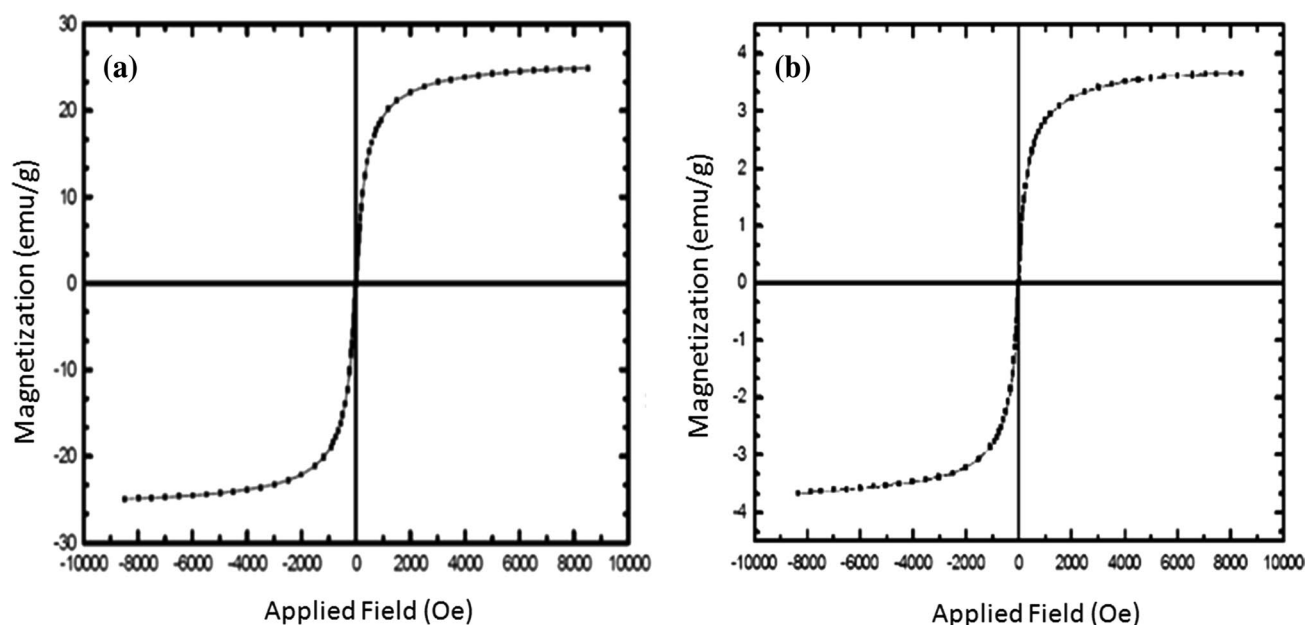


Fig. 14 VSM analysis of **a** $\text{Fe}_3\text{O}_4@/\text{SiO}_2$ and **b** $\text{Fe}_3\text{O}_4@/\text{SiO}_2\text{-Sb-Mo}$ (catalyst **3**) nanoparticles

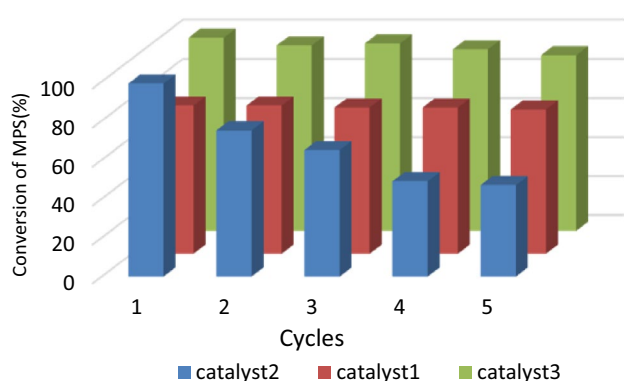


Fig. 15 Results of catalysts reuse experiments in the oxidation of methylphenyl sulfides. Reaction condition: sulfide (0.4 mmol), UHP (0.45 mmol), catalyst (0.01 mmol of molybdenum content), 0.5 mL CH_2Cl_2 , 0.5 mL MeOH, room temperature, 1 h

to 75% and then to 65%) due to the difficult separation of nanoparticles. Because of small size of particles, separation of this catalyst via filtration is not possible and part of catalyst seems to have been lost during time-consuming centrifugation. On the other hand, the magnetic catalyst **3** particles can be easily collected at the bottom of the test tube using a magnet and reused for five successive catalytic cycle with very slight loss of activity (99% first cycle, 90% fifth cycle). These results revealed that magnetic separation is more effective method than the conventional centrifugation (Fig. 15).

Due to the high catalytic activity and efficient recyclability of catalyst **3**, it was selected to study the substrate scope in the catalytic oxidation of sulfides to sulfoxides (Table 2). Using catalyst **3**, the oxidation of methylphenyl, ethylphenyl, diphenyl, dioctyl, and diethyl sulfide resulted

Table 2 Oxidation of sulfides by magnetic catalyst **3** in the presence of UHP

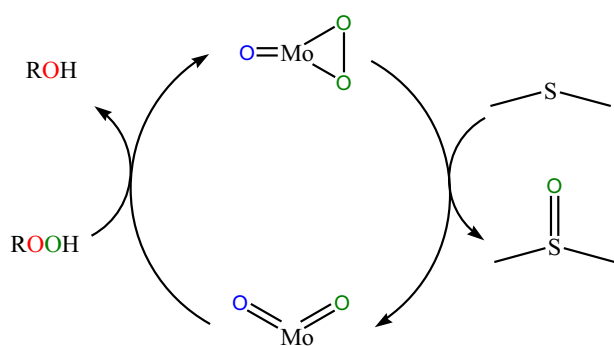


Entry	Substrate	Time (min)	Cycles	Conversion ^a (%)	Sel. to sulfoxide ^b (%)
1	Methylphenyl sulfide	30	1	> 99	95
2	Methylphenyl sulfide	30	2	98	96
3	Methylphenyl sulfide	30	3	96	95
4	Methylphenyl sulfide	30	4	95	94
5	Methylphenyl sulfide	30	5	90	91
6	Ethylphenyl sulfide	30	1	> 99	96
7	Ethylphenyl sulfide	30	2	> 99	96
8	Ethylphenyl sulfide	30	3	98	97
9	Ethylphenyl sulfide	30	4	> 99	97
10	Ethylphenyl sulfide	30	5	96	96
11	Diphenylsulfide	30	1	55	100
12	Diphenylsulfide	60	1	67	100
13	Diphenylsulfide	240	1	69	100
14	Diphenylsulfide	240	2	54	100
15	Diphenylsulfide	240	3	45	100
16	Dioctyl sulfide	60	1	55	100
17	Dioctyl sulfide	60	2	39	100
18	Diethyl sulfide	30	1	> 99	100
19	Diethyl sulfide	30	2	> 99	100
20	Diethyl sulfide	30	3	> 99	100
21	Diethyl sulfide	30	4	> 99	100

Reaction condition: sulfide (0.4 mmol), UHP (0.45 mmol), catalyst **1** (6.4 mg, 0.01 mmol of molybdenum content), 0.5 mL CH_2Cl_2 , 0.5 mL MeOH, room temperature

^aDetermined by GC using chlorobenzene as an internal standard

^bDetermined by GC, selectivity to sulfoxide = $T[\text{sulfoxide \%}/(\text{sulfoxide \%} + \text{sulfone \%})] \times 100$



Scheme 6 Suggested mechanism for the sulfide oxidation using UHP in the presence of catalyst

in the formation of corresponding sulfoxides in good yields (45–99%) and selectivities (91–100%). Control experiments indicated that no oxidation occurred in the absence of either catalysts or oxidant. In the other words, the use of $\text{Fe}_3\text{O}_4@$

SiO_2 , $\text{Fe}_3\text{O}_4@$ SiO_2 - NH_2 or $\text{Fe}_3\text{O}_4@$ SiO_2 -SB nanoparticles in place of catalyst **3** did not promote oxidation.

Scheme 6 shows a reasonable catalytic mechanism for oxidizing sulfides to sulfoxides, which is the first step of the mechanism involves the reaction between the molybdenum dioxo complex and UHP oxidant to produce oxo-peroxo compound and water. The nucleophilic attack of the sulfide on one oxygen atom of the peroxy ligand, yielding sulfoxide and regenerating the molybdenum(VI) dioxo complex, reenters the cycle [19].

The present catalytic system was also compared with the some reported catalysts (Table 3), and found that our nano-catalytic system ($\text{Fe}_3\text{O}_4@$ SiO_2 -SB-Mo) is superior to some reported catalytic protocols in terms of cost, reaction time, selectivity, conversion, and reusability [26, 39–45].

Table 3 Comparison of the activity of various catalysts in the oxidation of methyl phenyl sulfide

Entry	Catalytic system	Reaction condition	Reusability	Conversion (%)	Selectivity (%)	Yield (%)	References
1	Mo-oxazoline complex <i>cis</i> -[MoO ₂ (phox) ₂]	Urea–hydrogen peroxide, CH ₂ Cl ₂ /CH ₃ OH, 20 min, r.t.	–	95	100	–	[39]
2	Mo-DAPSH@APTES@SiO ₂	Hydrogen peroxide, solvent-free conditions, 0.5 h, r.t.	6	100	98	–	[26]
3	Oxo-peroxido Mo Schiff-base complex	Urea–hydrogen peroxide, CH ₃ OH/CH ₂ Cl ₂ , r.t., 35.25 min	–	100	96	–	[40]
4	Nano-magnetic-based <i>N</i> -propylsulfamic acid	Hydrogen peroxide, 80 min, r.t. solvent-free conditions	10	–	–	87	[41]
5	Silica-based tungstate inter-phase	Hydrogen peroxide, 90 min, CH ₃ OH/CH ₂ Cl ₂ r.t.	8	–	–	82	[42]
6	MoO ₂ Cl ₂	Hydrogen peroxide, acetone/water, 5 min, r.t.	–	–	–	96	[43]
7	[MoO ₂ (L)(CH ₃ OH)]	Urea–hydrogen peroxide, C ₂ H ₅ OH, r.t., 30 min	–	100	2	–	[44]
8	SiO ₂ -W2-Im(catalyst1)	Hydrogen peroxide, 2.5 h, CH ₃ OH/CH ₂ Cl ₂ , r.t.	6	97.9	–	91.9	[45]
9	This work	Urea–hydrogen peroxide, CH ₃ OH/CH ₂ Cl ₂ , r.t., 30 min	5	>99	95	95	This work

Conclusion

In summary, a Mo(VI) complex was immobilized on magnetic and non-magnetic supports. The obtained heterogenized catalysts were characterized with various characterization techniques, and their advantages and disadvantages in catalytic oxidation of sulfides were discussed. Among the tested catalysts, catalyst **1** with micro-size silica support showed the lowest catalytic activity. However, this catalyst can be recycled by simple filtration without any loss of catalytic efficiency. Although catalyst **2** (nano-SiO₂ support) exhibited the high efficiency in the first catalytic cycle, but its catalytic activity was significantly reduced in the next cycles due to the difficulties which arose in the course of the separation of catalysts particles. The Mo(VI) complex immobilized on silica-coated magnetic nanoparticles (catalyst **3**) was the best-performing catalyst for catalytic oxidation of sulfides under the experimental conditions investigated. In this application, the magnetic catalyst **3** has many advantages such as high conversions and selectivities, applicability to a wide range of sulfides, high loading value, and successful recycle of catalyst by simple magnetic separation.

Acknowledgements We are grateful to the Faculty of Chemistry of Bu-Ali Sina University for the financial support. We also acknowledge the Research Council of Sharif University of Technology for research funding of this project.

References

- M. Tajbakhsh, M. Farhang, S.M. Baghbanian, R. Hosseinzadeh, M. Tajbakhsh, *New J. Chem.* **39**, 1827 (2015)
- B. Yang, Z. Mao, X. Zhu, Y. Wan, *Catal. Commun.* **60**, 92 (2015)
- R. Mohammadi, E. Eidi, M. Ghavami, M.Z. Kassae, *J. Mol. Catal. A Chem.* **393**, 309 (2014)
- S. Shylesh, V. Schunemann, W.R. Thiel, *Angew Chem. Int. Ed.* **49**, 3428 (2010)
- C.H. Zhou, *Appl. Clay Sci.* **53**, 87 (2011)
- M. Gholinejad, A. Neshat, F. Zareh, C. Nájera, M. Razeghi, A. Khoshnood, *Appl. Catal. A Gen.* **525**, 31 (2016)
- V. Polshettiwar, R. Luque, A. Fihri, H. Zhu, M. Bouhrara, J. Basset, *Chem. Rev.* **111**, 3036 (2011)
- Z. Durmus, H. Erdemi, A. Aslan, M.S. Toprak, H. Sozeri, A. Baykal, *Polyhedron* **30**, 419 (2011)
- B. Sreedhar, A. Suresh-Kumar, P. Surendra-Reddy, *Tetrahedron Lett.* **51**, 1891 (2010)
- W. Li, B. Zhang, X. Li, H. Zhang, Q. Zhang, *Appl. Catal. A Gen.* **459**, 65 (2013)
- H. Woo, K. Lee, J.C. Park, K.H. Park, *New J. Chem.* **38**, 5626 (2014)
- M.S. Saeedi, S. Tangestaninejad, M. Moghadam, V. Mirkhani, I. Mohammadpoor-Baltork, A.R. Khosropour, *Polyhedron* **49**, 158 (2013)
- A. Rostami, B. Atashkar, *J. Mol. Catal. A Chem.* **398**, 170 (2015)
- E. Karaoglu, A. Baykal, M. Senel, H. Sozeri, M.S. Toprak, *Mater. Res. Bull.* **47**, 2480 (2012)
- Y.C. Chang, D.H. Chen, *J. Hazard. Mater.* **165**, 664 (2009)
- M. Bagherzadeh, L. Tahsini, R. Latifi, L.K. Woo, *Inorg. Chim. Acta* **362**, 3698 (2009)
- D.P. Debecker, D. Hauwaert, M. Stoyanova, A. Barkschat, U. Rodemerck, E.M. Gaigneaux, *Appl. Catal. A Gen.* **391**, 78 (2011)
- H. Zhang, G. Wang, *Tetrahedron Lett.* **55**, 56 (2014)
- H. Keypour, M. Balali, M.M. Haghdoost, M. Bagherzadeh, *RSC Adv.* **5**, 53349 (2015)
- Y. Yuan, N. Chen, R. Liu, S. Zhang, X. Liu, *Mater. Res. Bull.* **50**, 392 (2014)
- C. Hsu, P.Y. Hsu, Y.-L. Wub, W.-Y. Hsu, J.-J. Lin, *Appl. Surf. Sci.* **258**, 8641 (2012)
- J. Zhou, X. Chen, H. Duan, J. Ma, Y. Ma, *Appl. Surf. Sci.* **331**, 504 (2015)
- M. Bagherzadeh, M.M. Haghdoost, A. Shahbazirad, *J. Coord. Chem.* **56**, 591 (2012)
- M. Bagherzadeh, M.M. Haghdoost, F. Matloubi-Moghaddam, B. Koushki-Foroushani, S. Saryazdi, E. Payab, *J. Coord. Chem.* **66**, 3025 (2013)
- M.A. Zolfigol, A. Khazaei, M. Safaiee, M. Mokhlesi, R. Rostamian, M. Bagheri, M. Shiri, H. Gerhardus-Kruger, *J. Mol. Catal. A Chem.* **370**, 80 (2013)
- R.K. Sharma, A. Pandey, S. Gulati, *Polyhedron* **45**, 86 (2012)
- Y. Liu, B.Q., X. Li, X. Le, W. Zhang, J. Ma, *J. Mol. Catal. A Chem.* **406**, 65 (2015)
- M. Esmaeilpour, A.R. Sardariana, J. Javidi, *Appl. Catal. A Gen.* **445**, 359 (2012)
- M. Jafarzadeh, I.A. Rahman, C.S. Sipaut, *Synth. Met.* **162**, 466 (2012)
- J. Zhang, P. Jiang, Y. Shen, W. Zhang, X. Li, *Microporous Mesoporous Mater.* **206**, 161 (2015)
- C.W. Lim, I.S. Lee, *Nano Today* **5**, 412 (2010)
- M.Z. Kassae, H. Masrouri, F. Movahedi, *Appl. Catal. A Gen.* **395**, 28 (2011)
- M. Masteri-Farhan, N. Tayyebi, *J. Mol. Catal. A Chem.* **348**, 83 (2011)
- C. Guo, Y. Hu, H. Qian, J. Ning, S. Xu, *Mater. Character.* **62**, 148 (2011)
- I.D. Dobrea, C.E. Ciocan, E. Dumitriu, M.I. Popa, E. Petit, V. Hulea, *Appl. Clay Sci.* **104**, 205 (2015)
- S. Shylesh, J. Schweizer, S. Demeshko, V. Sch-nemann, S. Ernst, W.R. Thiel, *Adv. Synth. Catal.* **351**, 1789 (2009)
- Z. Li, C. Chen, E. Zhan, N. Ta, Y. Li, W. Shen, *Chem. Commun.* **50**, 4469 (2014)
- X. Cheng, X. Yu, Z. Xing, *J. Colloid. Interf. Sci.* **372**, 1 (2012)
- M. Bagherzadeh, L. Tahsini, R. Latifi, A. Ellern, L.K. Woo, *Inorg. Chim. Acta* **361**, 2019 (2008)
- M. Bagherzadeh, M. Amini, H. Parastar, H.M. Jalali, A. Ellern, L.K. Woo, *Inorg. Chem. Commun.* **20**, 86 (2012)
- A. Rostami, B. Tahmasbi, F. Abedi, Z. Shokri, *J. Mol. Catal. A Chem.* **378**, 200 (2013)
- B. Karimi, M. Ghoreishi-Nezhad, J.H. Clark, *Org. Lett.* **7**, 625 (2005)
- K. Jeyakumar, D.K. Chand, *Tetrahedron Lett.* **47**, 4573 (2006)
- I. Sheikshoae, A. Rezaiefard, N. Monadi, S. Kaafi, *Polyhedron* **28**, 733 (2009)
- S. Xian-Ying, W. Jun-Fa, *J. Mol. Catal. A Chem.* **280**, 142 (2008)